Supplementary Information: Maximum in density heterogeneities of active swimmers

Fabian Jan Schwarzendahl[1,2] and Marco G. Mazza[1]

[1] *Max-Planck-Institute for Dynamics and Self-Organization, Am Fassberg 17, 37077 Göttingen, Germany*
[2] *Georg-August-Universität Göttingen, Friedrich-Hund-Platz 1, 37077 Göttingen, Germany*

I. CHARACTERIZATION OF THE ACTIVE HYDRODYNAMICS

In the following we further characterize the fluid dynamics and the interactions mediated by the hydrodynamics in our microswimmer model.

A. Flow field scaling

In unbounded space, the fundamental solutions of the Stokes equation under point-like forcing has generally an algebraic decay with distance. It is therefore important to verify that our model reproduces such algebraic decay of the velocity over some interval of distances. Figure S1 shows the scaling behavior of the flow field behind both puller and pusher-type swimmers. In addition to the simulated data the theoretical prediction for a pusher (force dipole) and puller (three stokeslets), as well as the respective scalings are displayed. We find a good agreement with the theoretical prediction and the respective scaling laws.

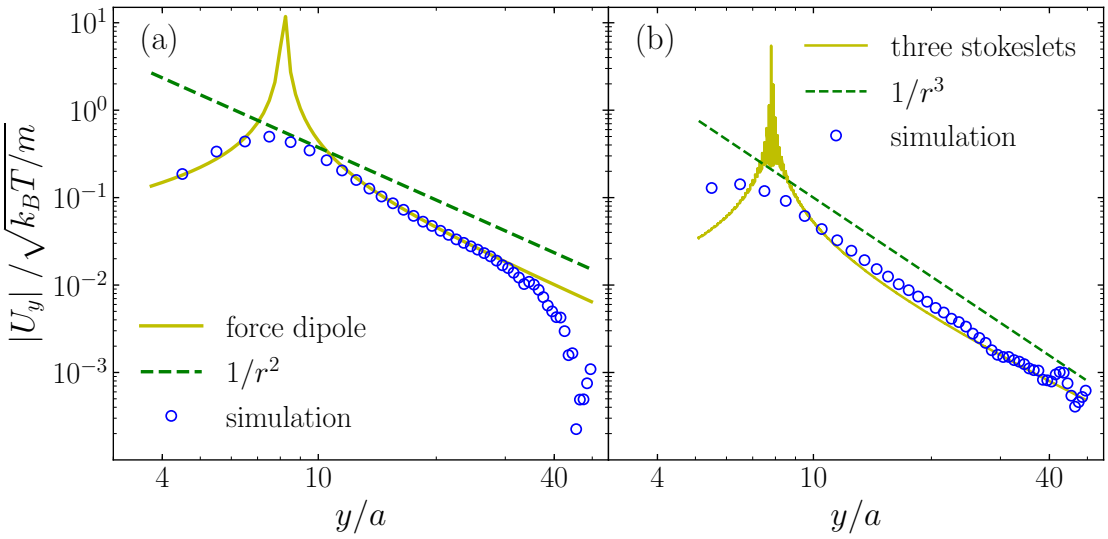

FIG. S1. Scaling behavior of the flow field behind (a) a pusher and (b) puller microswimmer. Blue circles show the numerical calculations, yellow continuous lines show the theoretical prediction of (a) a force dipole and (b) three Stokeslets, and green dashed lines show the expected power-law scaling for (a) $1/r^2$ and (b) $1/r^3$.

B. Two particle interactions

To characterize the two-particle interactions of our model, we first simulate two swimmers starting in a parallel configuration $\boldsymbol{e}_1 \cdot \boldsymbol{e}_2 = 1$, for initial center-of-mass (CoM) to center-of-mass distances $d_{\mathrm{CoM}} = 7a$ and $d_{\mathrm{CoM}} = 12a$. Second, we simulate two swimmers starting with a relative angle of $\pi/4$ and $\pi/2$, where the initial distance is $d_{\mathrm{CoM}} = 12a$.

In the following, we will show the time evolution of d_{CoM} as well as the orientational correlation function $\langle \cos\theta \rangle = \langle \boldsymbol{e}_1 \cdot \boldsymbol{e}_2 \rangle$ for both pusher and puller type swimmers. Additionally, we provide videos of each simulation to help understand the dynamics of the collisions.

a. Parallel configuration with $d_{\mathrm{CoM}} = 7a$. Figure S2(a) shows a scattering event between two pusher-type swimmers. The swimmers attract each other and stay in a parallel configuration until the steric interactions reorient them and they then start diverging from each other. Puller-type swimmers [Fig. S2(b)] immediately turn away from each other and perform a reorientation of an angle of π such that they are parallel again. Immediately after this, a secondary collision causes them to turn away from each other and start swimming into different directions. See also video `2_pusher_d7a.avi` for pushers, and video `2_puller_d7a.avi` for pullers.

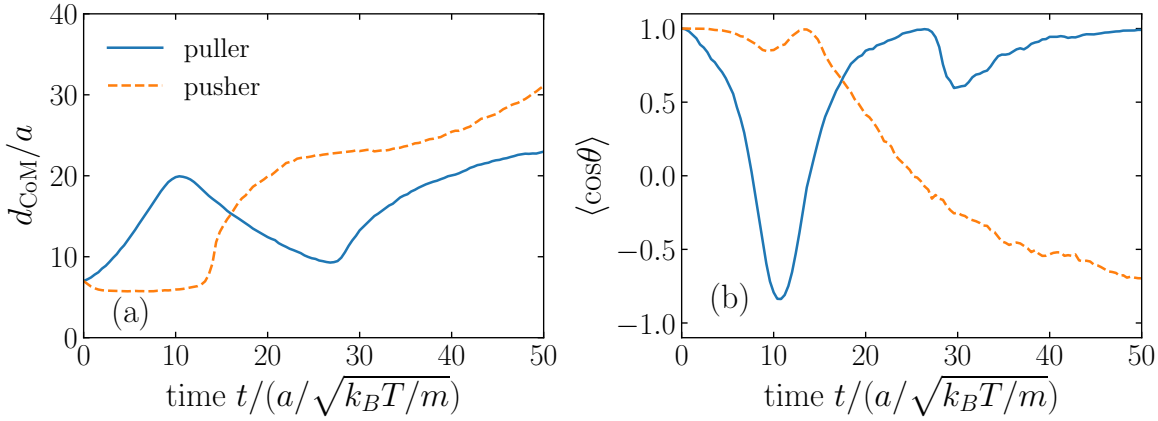

FIG. S2. Scattering event between two swimmers starting in a parallel configuration, with $d_{\mathrm{CoM}} = 7a$. Solid lines show puller and dashed lines pusher-type swimmers. (a) Center-of-mass to center-of-mass distance of the two swimmers. (b) Orientational correlation of the swimmers.

b. Parallel configuration with $d_{\mathrm{CoM}} = 12a$. Figure S3(a) shows a scattering event between two pusher-type swimmers. The pushers attract each other and stay in a parallel configuration until the steric interactions reorient them and they then start diverging from each other. Puller-type swimmers [Fig. S3(b)] quickly reorient away from each other and become parallel again, assuming a configuration in which one swimmer is behind the other.

For the same initial configuration we also computed the flow field, which can be seen in Fig. S4. The pusher-type swimmers have almost a stagnation point between them, which gives a relative attraction and corresponding flow lines favor a parallel configuration. This is in accordance with the behavior seen in Fig. S3(a) and the video `2_pusher_d12a.avi`. Puller-type swimmers exhibit a region with very high velocity between them, favoring a reorientation as seen by the orientational correlation function in Fig. S3. The configuration in which the swimmers are behind each other is assumed because of the very low flow velocity at the point $x = 0a$, $y = -10a$. See also video `2_pusher_d12a.avi` for pushers, and video `2_puller_d12a.avi` for pullers.

c. Relative angle $\pi/4$ with $d_{\mathrm{CoM}} = 12a$. Figure S5(a) shows a scattering event between two pusher-type swimmers. The pushers collide and turn away from each other because of a complex interplay of hydrodynamic and steric interactions. Puller-type swimmers [Fig. S5(b)] collide, immediately turn away from each other and swim into different directions. See also video `2_pusher_d12a_45deg.avi` for pushers and video `2_puller_d12a_45deg.avi` for pullers.

d. Relative angle $\pi/2$ with $d_{\mathrm{CoM}} = 12a$. Figure S6(a) shows a scattering event between two pusher-type swimmers. The pushers collide and turn away from each other because of a complex interplay of hydrodynamic and steric interactions. Puller-type swimmers [Fig. S6(b)] collide, immediately turn away from each other and swim into different directions. See also video `2_pusher_d12a_90deg.avi` for pushers and video `2_puller_d12a_90deg.avi` for pullers.

In summary, the behavior of pusher-type swimmers due to hydrodynamic interactions can be summarized by saying that they attract each other and align with each other. This behavior is expected, as it is shown experimentally by

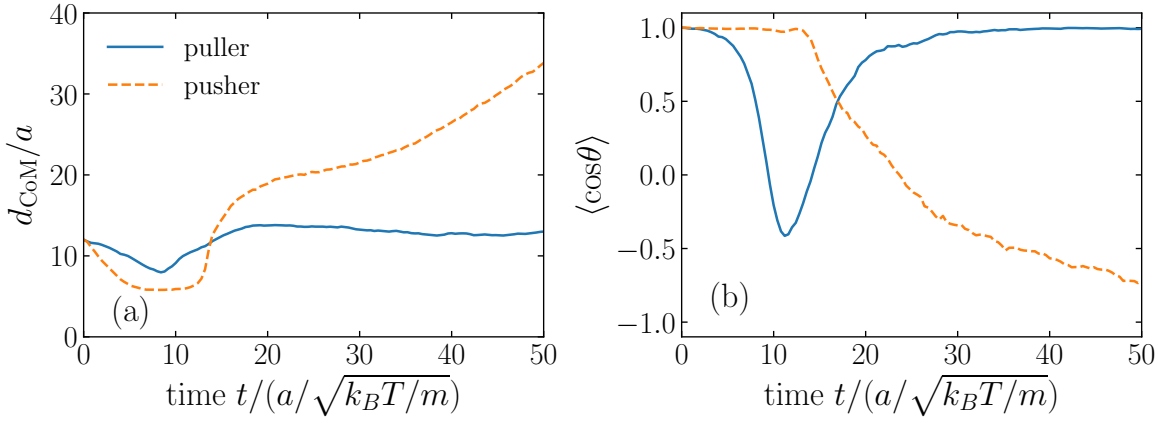

FIG. S3. Scattering event between two swimmers starting in parallel configuration, with $d_{\mathrm{CoM}} = 12a$. Solid lines show puller and dashed lines pusher-type swimmers. (a) Center-of-mass to center-of-mass distance of the two swimmers. (b) Orientational correlation of the swimmers.

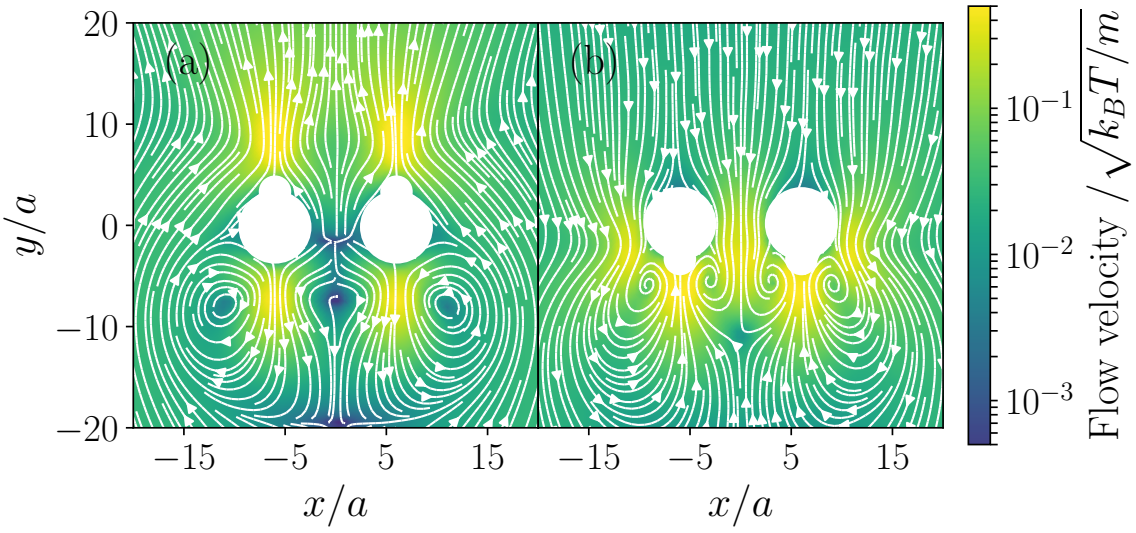

FIG. S4. Time-averaged flow field generated by (a) two model pushers (b) two model pullers. The swimmers are kept in a parallel configuration with $d_{\mathrm{CoM}} = 12a$. We show cross-sections on the x-y plane at $z = 0$. The force strength is $f_0 = 50k_{\mathrm{B}}T/a$. The large central white regions mark the hard cores of the active swimmers. The thin lines with arrows mark the streamlines, while the color code indicates the magnitude of the flow velocity normalized to the thermal velocity.

[1] and suggested by theoretical studies [2].

The behavior of puller-type swimmers due to their flow field can be summarized as generally dealigning. This behavior is also suggested by theoretical studies [2]. Interestingly, for an initially close-to-parallel alignment we observe a chain-like swimming behavior after the scattering event. This chain-like motion is mediated by the three-Stokeslet flow field.

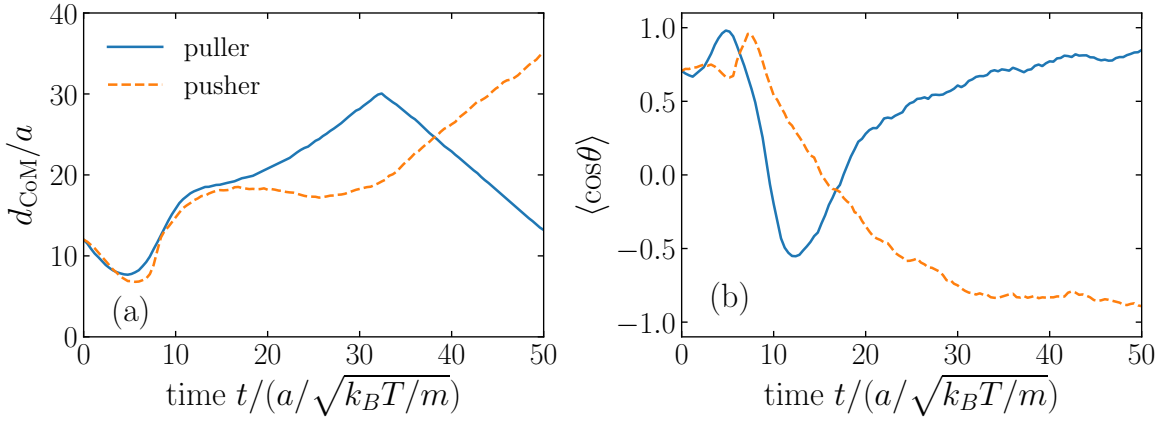

FIG. S5. Scattering event between two swimmers starting with a relative angle of $\pi/4$ and $d_{\mathrm{CoM}} = 12a$. Solid lines show puller and dashed lines pusher-type swimmers. (a) Center-of-mass to center-of-mass distance of the two swimmers. (b) Orientational correlation of the swimmers.

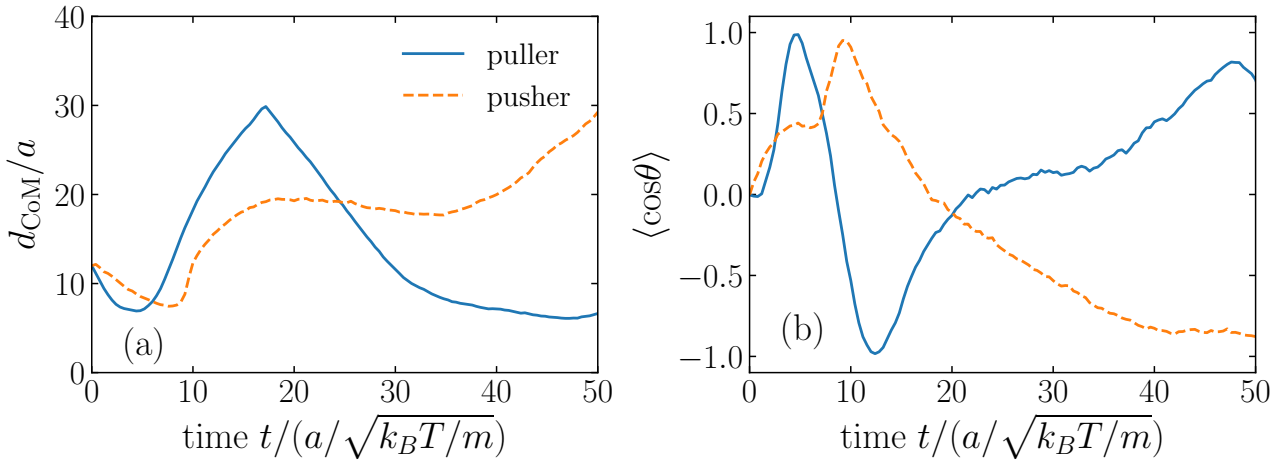

FIG. S6. Scattering event between two swimmers starting with a relative angle of $\pi/2$ and $d_{\mathrm{CoM}} = 12a$. Solid lines show puller and dashed lines pusher type swimmers. (a) Center-of-mass to center-of-mass distance of the two swimmers. (b) Orientational correlation of the swimmers.

II. RESULTS AT LOWER REYNOLDS NUMBER

To test the relevance of the Reynolds number on our results, we perform addition simulations with $N = 300 - 1560$ swimmers. Here, we use a smaller MPCD timestep of $\delta t = 2 \times 10^{-3}\sqrt{ma^2/(k_\mathrm{B}T)}$ and an average of $\langle N_\mathrm{C}\rangle = 5$ MPCD particles per cell. We note that the small value of MPCD timestep ensures that the fluid remains incompressible. The resulting Reynolds number is $\mathscr{R} = 10^{-3}$, and the Peclet number is $\mathscr{P} = 220$. Figure S7 shows the resulting standard deviation of local Voronoi volume σ_loc compared to standard deviation σ_rnd of a homogeneous configuration for both pullers and pusher. For both puller and pusher-type swimmers we find a maximum. Thus, the qualitative behavior of Fig. 5 in the main text is recovered. We conclude that in the tested regime the Reynolds number has only minor effects.

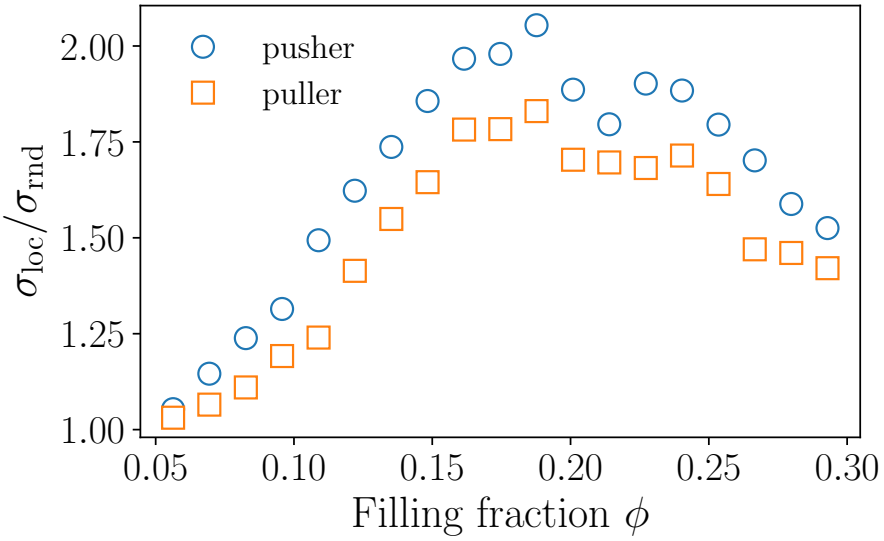

FIG. S7. Standard deviation of local Voronoi volume σ_loc compared to standard deviation σ_rnd of a homogeneous configuration. Global filling fraction is varied, the Péclet number is fixed to $\mathscr{P} = 220$ and the Reynolds number is $\mathscr{R} = 10^{-3}$. Circles are pusher and squares are puller-type swimmers.

III. BROWNIAN DYNAMICS SIMULATIONS

The Brownian dynamics simulations are carried out with hard spheres, that propel forward with a typical speed v_0 along their orientation $\boldsymbol{e}$ [see also [3–6]]. The equation governing the translational motion for the position $\boldsymbol{r}$ reads

$$\frac{\mathrm{d}\boldsymbol{r}}{\mathrm{d}t} = v_0\boldsymbol{e} + \boldsymbol{F}/\gamma + \boldsymbol{\eta}, \tag{S1}$$

where $\boldsymbol{F}$ is the force between particles and $\boldsymbol{\eta}$ is a random white noise with zero mean and $\langle\boldsymbol{\eta}(t)\boldsymbol{\eta}(t')\rangle = 2D\mathbf{I}\delta(t-t')$. Here, $D = k_\mathrm{B}T/\gamma$ is the translational diffusion constant, which is related to the friction coefficient γ. The potential between the particles is a Weeks–Chandler–Anderson potential [7]

$$\Phi(r_{ij}) = 4\tilde{\epsilon}\left[\left(\frac{\sigma}{r_{ij}}\right)^{12} - \left(\frac{\sigma}{r_{ij}}\right)^{6}\right] + \tilde{\epsilon} \tag{S2}$$

if $r_{ij} < 2^{1/6}\sigma$, and $\Phi(r_{ij}) = 0$ otherwise. Here $r_{ij} \equiv |\boldsymbol{r}_i - \boldsymbol{r}_j|$ is the distance between swimmer i and swimmer j and $\tilde{\epsilon} = 1000k_\mathrm{B}T$ is the energy scale. Furthermore, we include orientational diffusion by using

$$\frac{\mathrm{d}\boldsymbol{e}}{\mathrm{d}t} = \boldsymbol{\zeta} \times \boldsymbol{e} \tag{S3}$$

where $\boldsymbol{\zeta}$ is a Gaussian white noise with $\langle\boldsymbol{\zeta}(t)\boldsymbol{\zeta}(t')\rangle = 2D_r\mathbf{I}\delta(t-t')$. Here, the rotational diffusion coefficient is related to the translational diffusion coefficient by $D_r = 3D/\sigma^2$. The Péclet number is defined by $\mathscr{P} = v_0\sigma/D$, equivalently to the definition in the main text.

IV. MULTIPOLE EXPANSION OF HYDRODYNAMIC FORCES AND TORQUES

The hydrodynamic forces and torques in the analytical theory are approximated with two point forces. In addition, the correlations between noise and hydrodynamic interactions are neglected. Using these approximations, the velocities induced by swimmer 2 at the position of the front $\boldsymbol{r}_{L_1}$ and back $\boldsymbol{r}_{S_1}$ sphere of swimmer 1 are found from Eq. (10) in the main text and read

$$u_i\left(\boldsymbol{r}_{L_1}\right) = f\left[O_{ij}\left(\boldsymbol{r}_{L_1}-\boldsymbol{r}_{L_2}\right) - O_{ij}\left(\boldsymbol{r}_{L_1}-\boldsymbol{r}_{S_2}\right)\right]e_{2,j}, \tag{S4}$$

$$u_i\left(\boldsymbol{r}_{S_1}\right) = f\left[O_{ij}\left(\boldsymbol{r}_{S_1}-\boldsymbol{r}_{L_2}\right) - O_{ij}\left(\boldsymbol{r}_{S_1}-\boldsymbol{r}_{S_2}\right)\right]e_{2,j}, \tag{S5}$$

where O_{ij} is the Oseen tensor and $e_{2,j}$ is the orientation of swimmer 2. We now change coordinates in terms of the hydrodynamic center of the swimmers

$$\boldsymbol{e}_\mu = \left(\boldsymbol{r}_{L\mu}-\boldsymbol{r}_{S\mu}\right)/l, \tag{S6}$$

$$\boldsymbol{r}^C_\mu = \frac{a_L\boldsymbol{r}_{L,\mu}+a_S\boldsymbol{r}_{S,\mu}}{a_L+a_S}, \tag{S7}$$

where $\mu = 1,\ldots,N$ are particle indices. Equation (S4)-(S5) become

$$u_i\left(\boldsymbol{r}_{L_1}\right) = f\left[O_{ij}\left(\boldsymbol{r}^C_{12}+\frac{a_S l}{2\bar{a}}\left(\boldsymbol{e}_1-\boldsymbol{e_2}\right)\right) - O_{ij}\left(\boldsymbol{r}^C_{12}+\frac{l}{2\bar{a}}\left(a_S\boldsymbol{e}_1+a_L\boldsymbol{e_2}\right)\right)\right]e_{2,j}, \tag{S8}$$

$$u_i\left(\boldsymbol{r}_{S_1}\right) = f\left[O_{ij}\left(\boldsymbol{r}^C_{12}-\frac{l}{2\bar{a}}\left(a_L\boldsymbol{e}_1+a_S\boldsymbol{e_2}\right)\right) - O_{ij}\left(\boldsymbol{r}^C_{12}-\frac{a_L l}{2\bar{a}}\left(\boldsymbol{e}_1-\boldsymbol{e_2}\right)\right)\right]e_{2,j}, \tag{S9}$$

where $\bar{a} = (a_S+a_L)/2$. Equations (S8) and (S9) are now used to compute forces and torques between the particles

$$\begin{aligned}\partial_t\boldsymbol{r}^C_\mu &= \frac{a_L\partial_t\boldsymbol{r}_{L\mu}+a_S\partial_t\boldsymbol{r}_{S\mu}}{a_L+a_S}\\ &= \frac{a_L\boldsymbol{u}(\boldsymbol{r}_{L\mu})+a_S\boldsymbol{u}(\boldsymbol{r}_{S\mu})}{a_L+a_S}\\ &= \frac{1}{\zeta_{hy}}\sum_{\mu\neq\nu}\boldsymbol{F}_{\mu\nu},\end{aligned} \tag{S10}$$

$$\begin{aligned}\partial_t\boldsymbol{e}_\mu &= \left(\boldsymbol{e}_\mu\times\frac{\partial_t\boldsymbol{r}_{L\mu}+\partial_t\boldsymbol{r}_{S\mu}}{l}\right)\times\boldsymbol{e}_\mu\\ &= \left(\boldsymbol{e}_\mu\times\frac{\boldsymbol{u}(\boldsymbol{r}_{L\mu})+\boldsymbol{u}(\boldsymbol{r}_{S\mu})}{l}\right)\times\boldsymbol{e}_\mu\\ &= \frac{1}{\zeta_{hy}}\sum_{\mu\neq\nu}\boldsymbol{\tau}_{\mu\nu}\times\boldsymbol{e}_\mu,\end{aligned} \tag{S11}$$

where the last step in both Eq. (S10) and Eq. (S11) implicitly defines $\boldsymbol{F}_{\mu\nu}$ and $\boldsymbol{\tau}_{\mu\nu}$. In the orientational equation we projected on the perpendicular part of $\boldsymbol{e}_\mu$ because $|\boldsymbol{e}_\mu|^2 = 1$. Physically, this is related to the fact that the two spheres of one swimmer are connected by a stiff rod. The hydrodynamic friction coefficient is $\zeta_{hy} = \frac{1}{6\pi\eta\bar{a}}$. On account of the finite extension of our swimmers, we need to consider a multipole expansion of the force and torque defined in Eq.(S10)-(S11). The multipole expansion of the Oseen tensor is given by [8]

$$O_{ij}(\boldsymbol{r}+\boldsymbol{x}) = \sum_{n=0}^{\infty}\frac{1}{n!}\left(\boldsymbol{x}\cdot\nabla\right)^n O_{ij}(\boldsymbol{r}). \tag{S12}$$

We expand Eq.(S10)-(S11) up to $n = 2$, which correspond to neglecting terms of order $\mathscr{O}(\frac{1}{r^4})$. Therefore, we need the first two derivatives of the Oseen tensor, which are given by

$$\partial_k O_{ij} = \frac{1}{8\pi\eta}\left[\frac{1}{r^3}\left(-\delta_{ij}r_k + \delta_{jk}r_i + \delta_{ik}r_j\right) - \frac{3}{r^5}r_i r_j r_k\right], \tag{S13}$$

$$\begin{aligned}\partial_m\partial_k O_{ij} =& \frac{1}{8\pi\eta}\left[\frac{1}{r^3}\left(-\delta_{ij}\delta_{km} + \delta_{jk}\delta_{im} + \delta_{ik}\delta_{jm}\right)\right.\\ &\left. - \frac{3}{r^5}\left(-\delta_{ij}r_m r_k + \delta_{jk}r_m r_i + \delta_{ik}r_m r_j + \delta_{mi}r_j r_k + \delta_{jm}r_i r_k + \delta_{mk}r_i r_j\right) + \frac{15}{r^7}r_i r_j r_k r_m\right],\end{aligned} \tag{S14}$$

where $\partial_i \equiv \frac{\partial}{\partial r_i}$. Collecting all terms from the multipole expansion up to $\mathscr{O}(\frac{1}{r^4})$, we arrive at the following two-body expressions for force and torque

$$\boldsymbol{F}_{12} = \frac{9}{4}f\bar{a}l\frac{\hat{\boldsymbol{r}}_{12}}{r_{12}^2}S_{ij}(\hat{\boldsymbol{r}}_{12})e_{2i}e_{2j} - \frac{9}{16}fl^2\Delta a\frac{1}{r_{12}^3}\left[\hat{\boldsymbol{r}}_{12}S_{ijk}(\hat{\boldsymbol{r}}_{12})e_{2i}e_{2j}e_{2k} - \boldsymbol{e}_2 S_{ij}(\hat{\boldsymbol{r}}_{12})e_{2i}e_{2j}\right], \tag{S15}$$

$$\boldsymbol{\tau}_{12} = -\frac{9}{4}f\bar{a}l^3\left(\boldsymbol{e}_1 \times \hat{\boldsymbol{r}}_{12}\right)\frac{1}{r_{12}^3}S_{ijk}(\hat{\boldsymbol{r}}_{12})e_{2i}e_{2j}e_{2k}, \tag{S16}$$

where we used the symmetric traceless tensors

$$S_{ij}(\hat{\boldsymbol{r}}) = \left[\hat{r}_i\hat{r}_j - \frac{1}{3}\delta_{ij}\right], \tag{S17}$$

$$S_{ijk}(\hat{\boldsymbol{r}}) = 5\hat{r}_i\hat{r}_j\hat{r}_k - \left(\delta_{ik}\hat{r}_i + \delta_{ik}\hat{r}_j + \delta_{ij}\hat{r}_k\right), \tag{S18}$$

and summation over repeated indices is employed.

V. LINEAR STABILITY ANALYSIS

The Smoluchowski equation of our analytical model reads

$$\partial_t p = -\nabla\cdot\left[v(c)\boldsymbol{e}p\right] - \frac{1}{\zeta_{hy}}\nabla\cdot\left(\boldsymbol{F}_{hy}p\right) - \frac{1}{\zeta_{hy}l^2}\left(\boldsymbol{e}\times\frac{\partial}{\partial\boldsymbol{e}}\right)\cdot\boldsymbol{\tau}_{hy}p + D\Delta p + D_R\left(\boldsymbol{e}\times\frac{\partial}{\partial\boldsymbol{e}}\right)^2 p, \tag{S19}$$

where $p \equiv p(\boldsymbol{r}, \boldsymbol{e}, t)$, and the force and torque terms are computed using a mean field Ansatz

$$\langle X_{12}\rangle = \int \mathrm{d}\boldsymbol{r}_2 \int \mathrm{d}\boldsymbol{e}_2 X_{12} p(\boldsymbol{r}_2, \boldsymbol{e}_2, t). \tag{S20}$$

Using the definitions of the moments for, respectively, the concentration, polarization, and nematicity

$$c(\boldsymbol{r}, t) = \int \mathrm{d}\boldsymbol{e}\; p(\boldsymbol{r}, \boldsymbol{e}, t), \tag{S21}$$

$$\boldsymbol{P}(\boldsymbol{r}, t) = \frac{1}{c(\boldsymbol{r}, t)}\int \mathrm{d}\boldsymbol{e}\; \boldsymbol{e}\; p(\boldsymbol{r}, \boldsymbol{e}, t), \tag{S22}$$

$$\mathbf{Q}(\boldsymbol{r}, t) = \frac{1}{c(\boldsymbol{r}, t)}\int \mathrm{d}\boldsymbol{e}\left(\boldsymbol{e}\otimes\boldsymbol{e} - \frac{1}{3}\mathbf{I}\right)p(\boldsymbol{r}, \boldsymbol{e}, t), \tag{S23}$$

we can find the following expressions for the hydrodynamic force and torque terms

$$F_{hy,i} = \frac{9}{4}f\bar{a}lK_i^{F_1} + \frac{9}{16}fl^2\Delta a K_i^{F_2}, \tag{S24}$$

$$\tau_{hy,i} = -\frac{9}{4}f\bar{a}l^3\varepsilon_{imn}e_{1m}e_{1j}K_{nj}^{\tau}, \tag{S25}$$

with

$$K_i^{F_1} = \int \mathrm{d}\boldsymbol{r}_2 \frac{\hat{r}_{12i}}{r_{12}^2}S_{ij}(\hat{\boldsymbol{r}}_{12})c(\boldsymbol{r}_2, t)Q_{ij}(\boldsymbol{r}_2, t), \tag{S26}$$

$$K_i^{F_2} = \int \mathrm{d}\boldsymbol{r}_2 \frac{1}{r_{12}^3}S_{ij}(\hat{\boldsymbol{r}}_{12})c(\boldsymbol{r}_2, t)P_j(\boldsymbol{r}_2, t), \tag{S27}$$

$$K_{nj}^{\tau} = \int \mathrm{d}\boldsymbol{r}_2 \frac{\hat{r}_{12n}}{r_{12}^3}S_{ljk}(\hat{\boldsymbol{r}}_{12})c(\boldsymbol{r}_2, t)Q_{lk}(\boldsymbol{r}_2, t). \tag{S28}$$

We now compute moment equations using Eq. (S21)-(S23) for the Smoluchowski Eq. (S19)

$$\partial_t c = -\partial_i \left(v(c) c P_i\right) + D\Delta c - \frac{9 f \bar{a} l}{4\zeta_{hy}} K_i^{F_1} c + \frac{9 f l^2 \Delta a}{16 \zeta_{hy}} K_i^{F_2} c, \tag{S29}$$

$$\partial_t c P_i = -\partial_j \left(v(c) c Q_{ij}\right) - \frac{1}{3}\partial_i \left(v(c) c\right) + D\Delta c P_i - D_R c P_i - \frac{3lf}{40\pi\eta}\left(4K_{ij}^{\tau_1}(\boldsymbol{r},t) - K_{ji}^{\tau_1}(\boldsymbol{r},t) - \delta_{ij} K_{mm}^{\tau_1}(\boldsymbol{r},t)\right) c P_j \tag{S30}$$

$$\partial_t c Q_{ij} = -\frac{2}{5}\left(\partial_i v(c) c P_j\right)^{\mathrm{ST}} + D\Delta c Q_{ij} - 4 D_R c Q_{ij} - \frac{3lf}{8\pi\eta}\left[K_{ij}^{\tau}\right]^{ST} c, \tag{S31}$$

where we use the symmetric traceless part $[Y_{ij}]^{\mathrm{ST}} = \frac{1}{2}(Y_{ij} + Y_{ji}) - \frac{1}{3}\delta_{ij} Y_{kk}$. Note that here we neglected terms of order $\mathscr{O}(\mathbf{Q}^2)$. We will now linearize these moment equations around the isotropic state

$$\begin{aligned} c &= c_0 + \delta c\,, \\ \boldsymbol{P} &= \delta \boldsymbol{P}\,, \\ \mathbf{Q} &= \delta \mathbf{Q}\,, \end{aligned} \tag{S32}$$

and turn to Fourier space, where the fields are denoted by $\delta\tilde{c}$, $\delta\tilde{\boldsymbol{P}}$, and $\delta\tilde{\mathbf{Q}}$. First, note that all terms of order $\mathscr{O}(\boldsymbol{P}^2)$, $\mathscr{O}(\mathbf{Q}\boldsymbol{P})$, and $\mathscr{O}(\mathbf{Q}^2)$ will vanish at our level of approximation. Therefore, there is no contribution from hydrodynamic forces or torques in the polarization Eq. (S30). Second, the three terms proportional to $K_i^{F_1} c$ and $K_i^{F_2} c$, stemming from the concentration Eq. (S29), and the term proportional to $\left[K_{ij}^{\tau}\right]^{ST} c$ from the nematic stress tensor Eq. (S31) require special care in their evaluation. We will treat each of these three terms separately in the following.

A. $K_i^{F_1} c$ term

The linearized form of the $K_i^{F_1} c$ term is

$$\partial_i c_0^2 \int \mathrm{d}\boldsymbol{r}_2 \frac{\hat{r}_{12i}}{r_{12}^2} S_{ij}(\hat{\boldsymbol{r}}_{12}) \delta Q_{ij}(\boldsymbol{r}_2, t) \tag{S33}$$

and turning to Fourier space yields

$$i c_0^2 k_i \delta\tilde{Q}_{jk} \mathscr{F}\left[\frac{\hat{r}_i}{r^2}\left(\hat{r}_j\hat{r}_k - \frac{1}{3}\delta_{jk}\right)\right](k), \tag{S34}$$

where we used the convolution theorem, and $\mathscr{F}[h(\boldsymbol{r})](\boldsymbol{k}) = \int \mathrm{d}\boldsymbol{r} h(\boldsymbol{r}) e^{-i\boldsymbol{k}\cdot\boldsymbol{r}}$ denotes the Fourier transform of the function $h(\boldsymbol{r})$. Without loss of generality we can set $\boldsymbol{k} = k\boldsymbol{e}_z$, and using spherical coordinates gives

$$i c_0^2 \delta\tilde{Q}_{jk} \int_0^\infty \mathrm{d}\rho \int_0^{2\pi} \mathrm{d}\varphi \int_0^\pi \mathrm{d}\theta k \sin\theta \cos\theta \left(\hat{r}_j\hat{r}_k - \frac{1}{3}\delta_{jk}\right) e^{-ik\rho\cos\theta} = 0\,. \tag{S35}$$

B. $K_i^{F_2} c$ term

The linearized form of the $K_i^{F_2} c$ term is

$$\partial_i c_0^2 \int \mathrm{d}\boldsymbol{r}_2 \frac{1}{r_{12}^3} S_{ij}(\hat{\boldsymbol{r}}_{12}) \delta P_j(\boldsymbol{r}_2, t) \tag{S36}$$

turning to Fourier space and using the convolution theorem yields

$$i c_0^2 k_i \delta\tilde{P}_j \mathscr{F}\left[\frac{1}{r_{12}^3}\left(\hat{r}_i\hat{r}_j - \frac{1}{3}\delta_{ij}\right)\right](k). \tag{S37}$$

We can again set $\boldsymbol{k} = k\boldsymbol{e}_z$, and by using spherical coordinates we find

$$i c_0^2 \delta\tilde{P}_j \int_0^\infty \mathrm{d}\rho \int_0^{2\pi} \mathrm{d}\varphi \int_0^\pi \mathrm{d}\theta \frac{k}{\rho} \sin\theta \left(\hat{r}_j \cos\theta - \frac{1}{3}\delta_{j3}\right) e^{-ik\rho\cos\theta} = -\frac{8}{9}\pi c_0^2 k P_3. \tag{S38}$$

The integrals were solved using Mathematica (see also the supplementary file `Integrals_hydroTerms.pdf`).

C. $\left[K^{\tau}_{ij}\right]^{ST} c$ term

The term $\left[K^{\tau}_{ij}\right]^{ST} c$ in its linearized form reads

$$c_0^2 \left[\int \mathrm{d}\boldsymbol{r}_2 \frac{\hat{r}_{12i}}{r_{12}^3} S_{njm}(\hat{\boldsymbol{r}}_{12}) \delta Q_{nm}(\boldsymbol{r}_2, t) \right]^{ST}. \tag{S39}$$

Turning to Fourier space and using the convolution theorem gives

$$c_0^2 \delta\tilde{Q}_{nm} \mathscr{F}\left[\frac{\hat{r}_i}{r^3} S_{njm}\right](k). \tag{S40}$$

This can be evaluated when we use $\boldsymbol{k} = k\boldsymbol{e}_z$ and spherical coordinates

$$c_0^2 \delta\tilde{Q}_{nm} \int_0^{\infty} \mathrm{d}\rho \int_0^{2\pi} \mathrm{d}\varphi \int_0^{\pi} \mathrm{d}\theta \frac{1}{\rho} \sin\theta \hat{r}_i S_{njm} = c_0^2 \mathscr{M}_{ij}(\delta\tilde{Q}_{ij}), \tag{S41}$$

where the matrix $\mathscr{M}_{ij}(\delta\tilde{Q}_{ij})$ was evaluated using Mathematica (see also the supplementary file `Integrals_hydroTerms.pdf`) to be

$$(\mathscr{M}_{ij}) = \frac{4}{5}\pi \begin{pmatrix} -\frac{2}{3}\left(\delta\tilde{Q}_{2,2} + \delta\tilde{Q}_{3,3}\right) & \frac{2}{3}\delta\tilde{Q}_{2,1} & -\delta\tilde{Q}_{3,1} \\ \frac{2}{3}\delta\tilde{Q}_{2,1} & \frac{2}{3}\delta\tilde{Q}_{2,2} & -\delta\tilde{Q}_{3,2} \\ -\delta\tilde{Q}_{3,1} & -\delta\tilde{Q}_{3,2} & \frac{2}{3}\delta\tilde{Q}_{3,3} \end{pmatrix}. \tag{S42}$$

The linearized equations are then given by

$$\partial_t \delta\tilde{c} = -\left[ik_i \left(v_0 c_0 - \zeta c_0^2 + c_0^2 \frac{\Delta a l^2 f}{30\eta\bar{a}} \right) \delta\tilde{P}_i + D k_i k_i \delta\tilde{c} \right], \tag{S43}$$

$$\partial_t \delta\tilde{P}_i = -\left[ik_j \left(v_0 - \zeta c_0\right) \delta\tilde{Q}_{ij} + ik_i \frac{1}{3}\left(\frac{v_0}{c_0} - 2\zeta\right) \delta\tilde{c} + \left(D k_j k_j + D_R\right) \delta\tilde{P}_i \right], \tag{S44}$$

$$\partial_t \delta\tilde{Q}_{ij} = -\left[i\frac{2}{5}\left(v_0 - \zeta c_0\right) \left[k_i \delta\tilde{P}_j\right]^{ST} + \frac{3lf}{8\pi\eta} c_0 \mathscr{M}_{ij}(\delta\tilde{Q}_{ij}) + \left(4D_R + k_n k_n D\right) \delta\tilde{Q}_{ij} \right]. \tag{S45}$$

---

[1] I. S. Aranson, A. Sokolov, J. O. Kessler and R. E. Goldstein, *Phys. Rev. E*, 2007, **75**, 040901.
[2] E. Lauga and T. R. Powers, *Reports on Progress in Physics*, 2009, **72**, 096601.
[3] A. Wysocki, R. G. Winkler and G. Gompper, *EPL (Europhysics Letters)*, 2014, **105**, 48004.
[4] Y. Fily and M. C. Marchetti, *Phys. Rev. Lett.*, 2012, **108**, 235702.
[5] G. S. Redner, M. F. Hagan and A. Baskaran, *Phys. Rev. Lett.*, 2013, **110**, 055701.
[6] J. Bialké, T. Speck and H. Löwen, *Phys. Rev. Lett.*, 2012, **108**, 168301.
[7] J. D. Weeks, D. Chandler and H. C. Andersen, *J. Chem. Phys.*, 1971, **54**, 5237–5247.
[8] S. Kim and S. Karrila, *Microhydrodynamics: Principles and Selected Applications*, Dover Publications, 2005.